OPTOELECTRONICS AND ADVANCED MATERIALS – RAPID COMMUNICATIONS Vol. 9, No. 9-10, September – October 2015, p. 1273 - 1279

Effects of pH value and hydrothermal time on the structure and photocatalytic activity of monoclinic-scheelite $BiVO_4$

JI-GUO HUANG, BO WANG, SHUO PANG, XIN-YU ZHANG, XIN-YU YANG, XUE-TING GUO, XIAN-SHENG WANG*

Key Laboratory of Groundwater Resources and Environment, Ministry of Education, Jilin University, Changchun 130026, PR China

Bismuth vanadate powders were prepared by the hydrothermal method at different pH values and different hydrothermal time. The materials were characterized by XRD, SEM, XPS and UV-vis DRS. The photocatalytic performance was evaluated by the degradation of methylene blue. The effect of pH values and hydrothermal time on morphology and photocatalytic performance was discussed. The highest photocatalytic performance on the degradation of MB was observed under pH=1.0 and hydrothermal time=12h for ms-$BiVO_4$. It is concluded that the excellent photocatalytic activity of ms-$BiVO_4$ samples at low pH and short hydrothermal time was associated with lower band gap and unique morphology.

(Received April 24, 2015; accepted September 9, 2015)

Keywords: Monoclinic $Bivo_4$, Ph Value, Hydromothermal Time, Photocatalys Activity, Methylene Blue

1. Introduction

In recent years, much effort has been made to develop novel and effective semiconductor photocatalysts, which serve crucial issue in photocatalytic process [1-6]. However, the most widely used photocatalyst TiO_2 is only active under ultraviolet (UV) light which accounts for less than 5% in sunlight [7].Therefore, effective utilization of visible light has become one of the most difficult challenges in photocatalysis, and it is highly desirable to develop a phoocatalyst that can use visible light in high efficiency [8-10]. As for this aim, different strategies have been put forward to broadening the light absorption edge. The alternative option consists of the creation of new kind of semiconductors with small band gap which allows visible light absorption. Among these new families of visible active photocatalysts, bismuth vanadate has been widely reported to exhibit good photocatalytic properties. $BiVO_4$ which was firstly suggested by Kudo et al. is considered as a promising visible light-active semiconductor with a fairly strong oxidation power [11-13].

According to previous reports, $BiVO_4$ appears in three main crystalline phases: zircon-tetragonal (zt-$BiVO_4$), tetragonal-scheelite (ts-$BiVO_4$) and monoclinic-scheelite (ms-$BiVO_4$) [14,15]. Tetragonal $BiVO_4$ with a 2.9 eV band gap mainly possesses a UV absorption band. While the monoclinic scheelite $BiVO_4$ with a 2.4 eV band gap has both a visible-light absorption band and a UV absorption band. The UV bands observed in the tetragonal and monoclinic $BiVO_4$ are assigned to the band transition from O 2p to V 3d. Thus it is concluded the visible light absorption is due to the transition from a valence band (VB) formed by Bi 6s or a hybrid orbital of Bi 6s and O 2p to a conduction band (CB) of V 3d [2,16].

Additionally, the Bi-O band in monoclinic $BiVO_4$ is distorted which increases the separation efficiency of the photo-induced electrons and holes [17,18]. Therefore among the three crystal types of $BiVO_4$, monoclinic $BiVO_4$ exhibits much higher photocatalytic activity than the other two tetragonal phases. As a result it is extraordinarily significant to carry out research on the selective preparation of monoclinic $BiVO_4$. Different types of $BiVO_4$ can be synthesized through different preparation routes which allow selectively obtaining one of the mentioned structures depending on the preparation method [19-21]. As for the photoactive monoclinic structure, it is usually obtained by means of high temperature methods. The tetragonal form is normally achieved by aqueous media methods at low temperature process. The $BiVO_4$ which is prepared by means of hydrothermal treatments at mild temperatures shows lower crystallite sizes, compared with those obtained from solid state reaction [22,23]. Plenty of preparation techniques have been investigated including solid state [24], combustion [25], aqueous processes such as hydrothermal [26], polymer assisted coprecipitation [27], flame process [28], and spray pyrolysis [29]. However, among these studies on the synthesis of $BiVO_4$ powders, the effect of pH values and hydrothermal time on crystalline phase, morphology, and photocatalytic performance of the powders have been barely reported.

Consequently, researching into the impact of pH values and hydrothermal time on morphology and photocatalytic performance of the powders is the priority goal in this study. Besides, $BiVO_4$ monoclinic systems obtaining with controlled morphology and the further photocatalytic activity for C_{MB} degradation have also been performed.

2. Experimental

2.1. Synthesis of photocatalysts

The preparation of Bi-based photocatalysts were carried out using the corresponding amounts of $Bi(NO_3)_3{\cdot}5H_2O$,and NH_4VO_3 as precursors. First, 10 mmol of Bi precursor was dissolved in dilute nitric acid (20ml) while amount of NH_4VO_3 (10mmol) was dissolved in sodium hydroxide solution (20ml).Then, these two solutions were mixed to form a yellowish suspension. After that the formed suspension was kept stirring for 30 min. Thirdly, the suspension was transferred into a Teflon recipient which was placed inside of stainless steel autoclave for hydrothermal treatment. Beforehand, the suspension was controlled at pH = 1, 4, 7 and 10 by respectively adding the appropriate amount of sodium hydroxide solution. The hydrothermal treatment was controlled at 180 ^oC for 12, 24, 36 and 48 h, separately. Forth, all the prepared photocatalysts were repeatedly washed and centrifuged followed by drying at 80 ^oC. At this stage, the catalysts by hydrothermal method was completed which are named as *H x-T* where x and T denote the pH value and the hydrothermal time, respectively.

2.2. Materials characterization

The sample morphology and surface elemental content were examined using a scanning electron microscope (FE-SEM, Model JEOL, JSM-6700F) equipped with energy dispersive X-ray spectroscopy (EDX, Rigaku Corporation). X-ray diffraction (XRD) spectra were obtained by a powder X-ray Diffractometer (RINT 2500, Rigaku Corporation, Japan) using Ni-filtered Cu Kα radiation in the range of 2θ from 10^o to 90^o. The crystallite size was obtained using MDI Jade 6.0. X-ray photoelectron spectroscopy (XPS) patterns were measured using X-ray photoelectron spectroscopy (Thermo, ESCALAB 250) to analyze the surface components with Al Kα radiation, and all spectra were referenced by setting the hydrocarbon C1s peak to 285.0 eV to compensate for residual charging effects. The UV-vis absorption spectra were recorded on a UV –vis spectrophotometer (Shimadzu, Model UV-2550) in the wavelength range of 200-800nm.

2.3. Photocatalytic degradation of MB

The MB photocatalytic degradation experiments were conducted in a batch reactor with a 500W Xenon lamp. The intensity of the incident light on the solution surface was controlled at 10000 Lux. The blank experiment was performed without catalyst and dye degradation was not observed after 2 h. In a typical MB photocatalytic degradation experiment, prior to the commencement, a 100 mL suspension containing 0.1 g photocatalysts (dosage = 1 g/L) and MB (10 mg/L) was prepared under magnetically stirred in darkness for 30 min to attain adsorption/desorption equilibrium. After equilibrium, the Xenon lamp was switched on. At designated time intervals, aliquots of the solution were centrifuged using centrifugal machine (Model TGL-16C) and subsequently analyzed using a spectrophotometer (Model UNICO 2100 visible) at 664 nm. In the case for MB, the dye discoloration proceeds by chromophore cleavage since no significant shift was observed in its characteristic UV-vis band followed the photoactivity study.

3. Results and discussion

3.1 XRD analysis

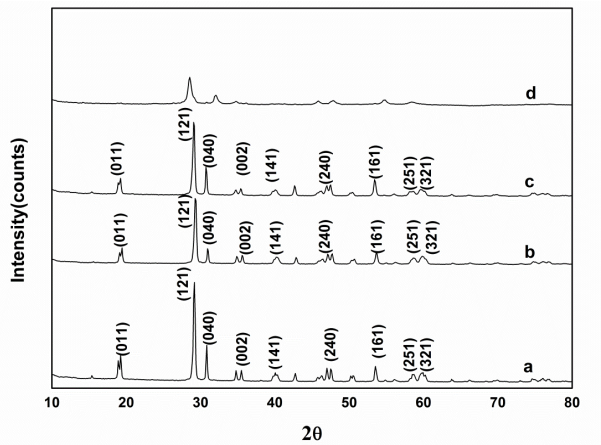

Fig. 1. XRD patterns of $BiVO_4$ powders prepared by hydrothermal method at the same hydrothermal time (12h) and different pH values : (a) pH=1, (b) pH=4, (c) pH=7 and (d) pH=10.

The XRD patterns of the $BiVO_4$ samples prepared at different conditions are shown in Fig.1. Hydrothermal treatment leads to single monoclinic phase in three series (*H 1*, *H 4* and *H 7*), but in *H 10* Bi_2O_3 and $Bi_2VO_{5.5}$ are slightly observed. When the pH value of the precursor was 1, $Bi(NO_3)_3{\cdot}5H_2O$ was hydrolyzed (as shown by reactions 3-1 and 3-2)

$$Bi^{3+} + H_2O \longleftrightarrow Bi(OH)^{2+} + H^+ \longleftrightarrow Bi(OH)^{2+} + 2H^+ \quad (3-1)$$

$$NO_3^- + Bi(OH)_2^+ \rightarrow BiONO_3\downarrow + H_2O \quad (3-2)$$

More H^+ species and a small amount of slightly soluble $BiONO_3$ was generated [30-32], little $BiVO_4$ was formed, as shown in reaction 3-3.

$$BiONO_3 + VO_3^- \rightarrow BiVO_4 \downarrow + NO_3^- \quad (3-3)$$

Zhou et al. found it was easy to generate the monoclinic sheelite $BiVO_4$ (ms-$BiVO_4$)) crystals with high crystallinity, because ms-$BiVO_4$ was thermodynamically more stable than the polymorph with the tetragonal zircon structure (tz-$BiVO_4$) under strong acidic conditions (pH≤0.59) [33]. Tan et al. found that the formation of tz-$BiVO_4$ was feasible kinetically when pH increase [34]. However, tz-$BiVO_4$ peaks for all the as-prepared samples were not obviously recognized. As the pH increased from 1 to 7, pure ms-$BiVO_4$ was obtained, as shown in Fig. 1. This could be ascribed to that the H^+ species were consumed gradually as the pH values increased, which induced the reversible reaction equilibrium to the right direction, as shown earlier in reactions 3-1 and 3-2. Therefore, when pH ≥ 1, the amount of $BiONO_3$ became greater and the generated amount of $BiVO_4$ also increased. Furthermore, as a mineralizer, OH^- forced the generation of tz-$BiVO_4$ at the first stage (pH ≤ 0.59) and the following transformation to ms-$BiVO_4$ via a dissolution-recrystallization process [35]. What's more, NaOH could determine the concentration of the monomer in the solution, adjust the nucleation rate and crystal growth rate of $BiVO_4$ [12], making the crystals generate stable monoclinic. In addition, it was observed that the peaks for ms-$BiVO_4$ crystals first showed very high and then became weakened. This observation means the ms-$BiVO_4$ crystals first showed enhanced crystallinity and then a weakened tendency toward crystallization when influenced by the increased amount of OH^-. Thus, the samples of pH=1 have high photocatalytic efficiency due to their distinct monoclinic phase structure and high intensity. At pH = 10, the peaks corresponding to Bi_2O_3 and $Bi_2VO_{5.5}$ appeared. Under alkaline conditions, the Bi^{3+} species could be easily hydrolyzed and aggregated to form the high polymer (seen in reaction 3-4):

$$nBi^{3+} + 2nOH^- \rightarrow [BinOn]_n^+ + nH_2O \quad (3-4)$$

The high polymer was dissolved to generate Bi_2O_3.

As shown in SFig. 1, the effect of hydrothermal treatment time on the $BiVO_4$ crystallinity is also be tested. The crystal sizes for as-synthesized samples were listed in Table 1 and were calculated from Scherrer equation:

$$Lc = K\lambda/\beta\cos\theta \quad (3-5)$$

Lc is the crystal size, λ is 0.15418nm,K=0.89, β=(FWHM/180°)×3.14 and 2θ=28.9°.

The crystal size for $BiVO_4$ became smaller with pH increase from 1 to 7 and finally reached minimum for Bi_2O_3. In addition, the crystal size nearly remained constant at 27.86, 24.20, 24.70 and 14.92 nm (Table 1) corresponding to pH 1, 4, 7 and 10, respectively. Comparing the crystallite size of these samples, it can be noticed that the preparation at longer hydrothermal time seems to induce slightly higher crystallite sizes. It can be deduced that as the hydrothermal time increases, an improvement in the crystallinity is achieved without changing the crystalline structure(Fig.2).

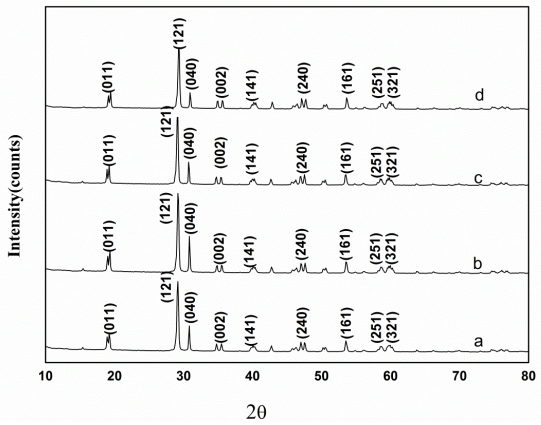

Fig. 2. XRD patterns of $BiVO_4$ powders prepared by hydrothermal method at the same pH value (pH=1) and different hydrothermal times: (a) 12h (b) 24h (c) 36h (d) 48h.

By observing the relationship between the different diffractions corresponding to (011), (040) and (002) planes, it is possible to infer that *H 1* and *H 7* series showed a clear preferential orientation for (040) plane (Table 1). On the contrary, for *H 4*, it appeared that (011) plane exhibited a relatively higher intensity comparing to the theoretical one. At the same time, the $I_{(040)} / I_{(121)}$ ratio appeared to be notably shrunken. The effect was related with the anisotropic growth of the particles which showed an acicular morphology.

3.2 Effect of pH

Fig. 3 shows SEM images of $BiVO_4$ powders prepared via the hydrothermal method at different pH values. As shown in Fig. 3a, the prepared polyhedral $BiVO_4$ at pH 1 showed irregular polyhedron. Normally, after the supersaturation of the precursor solution, the ms-$BiVO_4$ particles would nucleate. And then polyhedral crystals would be formed after the continuous monomer precipitation on the ms-$BiVO_4$ crystal nuclei. Similarly to the Fig. 3a, the prepared $BiVO_4$ at pH 4 also exhibited polyhedral crystal, but smaller size. This is consistent with the above XRD analysis. When furthering adding NaOH, pH in the precursor solution increased to 7, both of irregular polyhedral crystal and loose sphere profile appeared. It meant the morphology transformation from irregular polyhedral crystal to loose sphere took place. With the high pH=7, the edges of ms-$BiVO_4$ could be dissolved, thus resulted in smaller particles. In addition, NaOH consumed H^+ and pushed the reversible reactions (3-1, 3-2 and 3-3) equilibrium to the right direction. As a

consequence, much more amount of intermediate products during the above reactions was used for the formation of crystal seed, and less could be applied for forming monomer and decreased crystal growth. These discussions could explain the loose sphere profile was composed of small polyhedral crystal. When pH increased to 10, phase transformation occurred and the $Bi_2VO_{5.5}$ and Bi_2O_3 crystal took place of ms-$BiVO_4$. As discussed in XRD analysis, alkaline conditions could lead to Bi^{3+} species hydrolyzing. Therefore, besides the composition of $Bi_2VO_{5.5}$, Bi_2O_3 was formed. It should be noticed that the crystal size at pH 10 was the smallest in all of the as-prepared samples, but not the best photocatalytic performance. The first, high pH value would promote the nucleation rate and weaken the crystal growth rate, thus result in a smallest size. The second, Bi^{3+} species hydrolyzing would cause the stoichiometric imbalance for the reaction 3-2. And this was adverse for the formation of $BiVO_4$. Furthermore, the small crystal grains easily aggregated (seen in Fig. 3d). This aggregation could be responsible for the decreased photocatalytic activity.

It indicated that pH value has a great influence on the crystal phase, shape, and size of the final product, and high pH was not beneficial for the generation of ms-$BiVO_4$. Similar phenomenon was also reported in the literature which demonstrated that pH value of the reaction system had a significant influence on morphology, structures and the growth processes of $BiVO_4$ nanostructures [34].

We can demonstrate the effect of pH value on the crystal characteristics from how the pH influence the reversible reactions (3-1, 3-2 and 3-3). Acid conditions would result in high concentration of free Bi^{3+}, and thus lead to favorable crystal growth and good crystallinity. With the increase of pH value from 1 to 7, Bi^{3+} species were consumed so that nucleation rate was higher than crystal growth rate, which result in a relative smaller crystal size. When pH increased to 10, OH^- promoted hydrolysis of $Bi(NO_3)_3$ and thus led to the formation of Bi_2O_3 and mixed crystal.

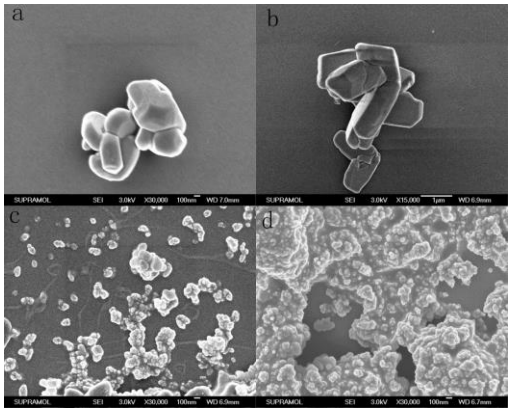

Fig. 3. SEM images of $BiVO_4$ samples prepared from hydrothermal method at the same hydrothermal time (12h) and different pH values: (a) pH=1, (b) pH=4, (c) pH=7 and (d) pH=10.

3.3 XPS analysis

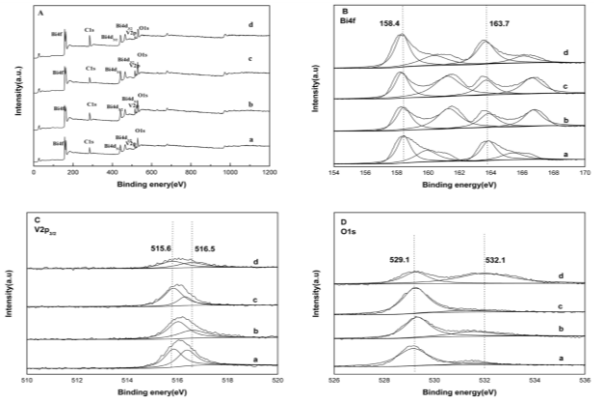

Fig. 4. (A)overall (B) Bi 4f (C) V2$p_{3/2}$ (D) O1s XPS spectra of $BiVO_4$ samples prepared at the same hydrothermal time (12h) and different pH values: (a) pH=1, (b) pH=4, (c) pH=7 and (d) pH=10.

The overall and elements XPS spectra for the ms-$BiVO_4$ are shown in Fig.4. From the wide scan XPS spectra (Fig. 4A) of the $BiVO_4$ samples, one can see that the XPS signals of Bi, V, O, and C were detected. It was observed from Figure 4B that the Bi 4f spectrum showed two sets of spin-orbit doublet peaks of the Bi $4f_{5/2}$ (158.4-161.3 eV) and Bi $4f_{7/2}$ (163.7-166.7 eV) signals [36]. The binding energies of Bi 4f spectrum for as-synthesized samples were listed in Table 2. For all the prepared $BiVO_4$ samples, the components of Bi spectrum included the two peaks at 158.4 and 163.7 eV, which were assigned both corresponding to Bi^{3+} species. Besides, the left 4f doublets at 159.8-161.3 eV and 165.3-166.7 eV were attributed to the surface Bi^{5+} species [37-39]. As the pH increased from 1 to 7, the peaks at 158.4 and 163.7 eV became weaker and smaller, while, the other peaks corresponding to Bi^{5+} became sharper and stronger. The result showed that the OH^- could catch the electrons of Bi oxide and convert some Bi^{3+} ions to Bi^{5+} ions, and thus resulted in ms-$BiVO_4$ crystallinity loss (corresponding to XRD results). However, when pH increased from 7 to 10, the peaks at 158.4 and 163.7 eV became sharper, while, other peaks became weaker. This was because Bi_2O_3 began appearing at pH 10. Figure 4C showed the V $2p_{3/2}$ XPS spectra of samples. The V $2p_{3/2}$ spectrum of each sample could be decomposed into two components at BE 515.6 and 516.5 eV, corresponding to the surface V^{4+} and V^{5+} species [40,41]. This result indicated that surface V^{4+} and V^{5+} species co-existed in these samples. Such a V $2p_{3/2}$ spectral feature are common in monoclinic $BiVO_4$ [3]. As shown in Fig. 4D, there were two components at BE 529.1 and 532.1 eV, assignable to the surface lattice oxygen (O_{latt}) and adsorbed oxygen (O_{ads}, e.g., O^-, O_2 or O_2^{2-}) [42, 43].

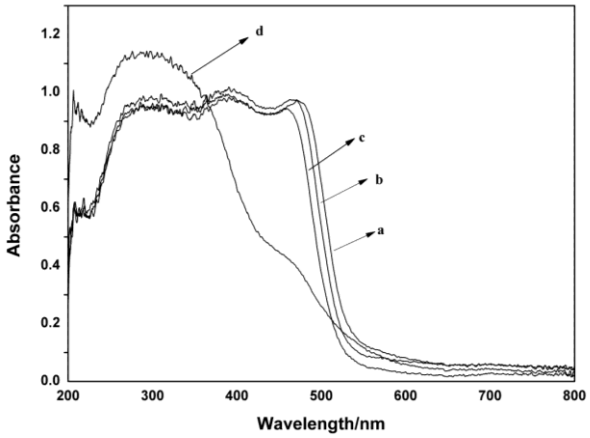

Fig. 5. UV-vis DRS spectrum of $BiVO_4$ samples prepared at the same hydrothermal time (12h) and different pH values: (a) pH=1, (b) pH=4, (c) pH=7 and (d) pH=10.

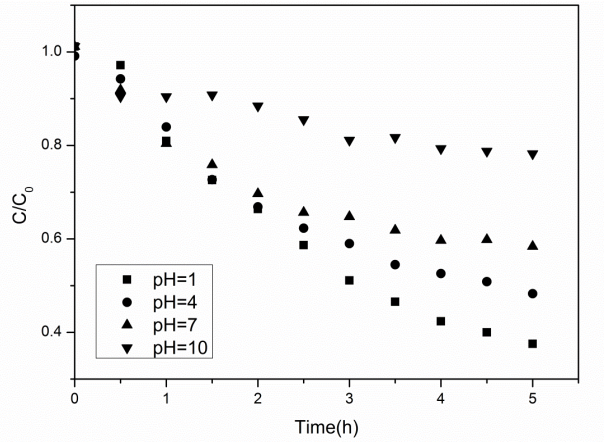

Fig. 6. Photocatalytic degradation of MB (initial concentration 10mg/L) versus simulated sunlight irradiation time (500W Xenon lamp, the intensity of the incident light on the solution surface was controlled at 10000 Lux), using $BiVO_4$ samples（catalyst dosage 1g/L）prepared at the same hydrothermal time (12h) and different pH values via hydrothermal method.

Table 1. Crystal size and structural characterization for synthesized samples.

Sample			Crystal size(nm)	I(011)/I(121)	I(040)/I(121)	I(002)/I(121)
12h	H	pH=1	27.86	0.238	0.353	0.127
		pH=4	24.20	0.232	0.219	0.121
		pH=7	24.70	0.217	0.373	0.084
		pH=10	14.92	-	-	-
24h	H	pH=1	27.86	0.252	0.449	0.09
		pH=4	24.20	0.277	0.219	0.108
		pH=7	25.5	0.195	0.333	0.091
		pH=10	16.27	-	-	-
36h	H	pH=1	27.74	0.274	0.325	0.105
		pH=4	24.20	0.233	0.219	0.104
		pH=7	26.417	0.153	0.154	0.105
		pH=10	15.526	-	-	-
48h	H	pH=1	27.38	0.275	0.282	0.129
		pH=4	26.10	0.302	0.218	0.103
		pH=7	26.31	0.189	0.422	0.089
		pH=10	23.1	-	-	-

Table 2. Binding energies for components of Bi 4f spectrum.

Samples	$Bi4f_{7/2}$	$Bi4f_{7/2}$	$Bi4f_{5/2}$	$Bi4f_{5/2}$
H 1-12	158.4	159.9	163.8	165.3
H 4-12	158.5	161.3	163.8	166.7
H 7-12	158.4	161.2	163.7	166.6
H 10-12	158.3	160.3	163.7	166.1

3.4 DRS analysis

The UV-vis DRS of polycrystalline and $BiVO_4$ samples are shown in Figure 5. All the samples showed very strong absorption in the UV-light region, but not in the visible-light region. The samples prepared at pH = 1, 4 and 7 from hydrothermal method showed absorption edge in the visible-light regions for 538, 530, 520 nm, respectively. At pH 10, the absorption curve of the as-prepared samples showed the apparent step-like within regions of 430−520 nm, which was related to its

mixed-phase structure: $BiV_2O_{5.5}$ and Bi_2O_3, as discussed in XRD and SEM analysis. The band gaps estimated by extrapolating the linear region of a plot of the absorbance squared vs energy[44] are 2.30, 2.33, 2.38 and 2.56 eV for *H1-12*, *H4-12*, *H7-12* and *H10-12*, respectively. These results were similar to the previous reports [45, 46] and indicated the electronic structure of $BiVO_4$ was changed as the crystalline phase changed.

3.5 Photocatalytic activity

The variation of MB concentration(C/C_0) with irradiation time over the different $BiVO_4$ samples was shown in Fig. 6, where C_0 is the initial concentration of MB solution before irradiation and C is the concentration of MB at t time. As shown in Fig. 6, the $BiVO_4$ samples prepared at pH 1 exhibited the best photocatalytic degradation of 63% for MB after 5 h visible light irradiation. And with the pH from 1 to 10, the photodegradation of MB by $BiVO_4$ samples decreased from 63% to 19%. This is because the loss of ms-$BiVO_4$ crystallinity from pH 1 to 7 and the replacement by Bi_2O_3 and $Bi_2VO_{5.5}$, which is demonstrated by XRD and XPS analysis. Generally, photocatalytic activities decreased with the increase of the particle size. But the $BiVO_4$ samples prepared at pH 1 showed the broader light adsorption edge than any other $BiVO_4$ samples. And this may be assigned to the best photocatalytic performance for $BiVO_4$ prepared pH at 1.

4. Conclusion

In summary, $BiVO_4$ powders have been prepared via the hydrothermal method, and their photocatalytic activities were investigated. It is found that the $BiVO_4$ with different crystal phases and morphologies can be prepared by varying the pH values and hydrothermal time of the precursors. As the pH increased from 1 to 7, pure ms-$BiVO_4$ was obtained. When pH increased to 10, phase transformation occurred and the $Bi_2VO_{5.5}$ and Bi_2O_3 crystal took place of ms-$BiVO_4$, the OH^- could catch the electrons of Bi oxide and convert some Bi^{3+} ions to Bi^{5+} ions, and thus resulted in ms-$BiVO_4$ crystallinity loss. The electronic structure of $BiVO_4$ was changed as the crystalline phase changed. The $BiVO_4$ samples prepared at pH 1 exhibited the best photocatalytic degradation of 63% for MB after 5 h visible light irradiation. It is concluded that the excellent photocatalytic activity of ms-$BiVO_4$ samples is at low pH and short hydrothermal time.

Acknowledgement

This work was supported by analysis and testing foundation of Jilin University and the National Natural Science Foundation of China (No. 51308252).

References

[1] D. J. Yang, C. C. Chen, Z. F. Zheng, H. W. Liu, E. R. Waclawik, Z. M. Yan Y. N. Huang, H. J. Zhang, J. C. Zhao, H. Y. Zhu, Energy Environ. Sci. **4**, 2279 (2011).
[2] F. Lu, W. P. Cai, Y. G. Zhang, Adv. Funct. Mater **18**, 1047 (2008).
[3] H. Y. Jiang, H. X. Dai, X. Meng, K. M. Ji, L. Zhang, Appl. Catal. B: Environ **105**, 326 (2011).
[4] D. G. Wang, R. G. Li, J. Zhu, J. Y. Shi, J. F. Han, X. Zong, C. Li, J. Phys. Chem. C **116**, 5082 (2012).
[5] W. J. Li, D. Z. Li, Y. M. Lin, P. X. Wang, W. Chen, X. Z. Fu, Y. Shao, Phys. Chem. C **116**, 3552 (2012).
[6] Y. F. Zhang, G. F. Li, X. H. Yang, H. Yang, Z. Lu, R. Chen, J. Alloys Compd **551**, 544 (2013).
[7] M. Y. Liu, W. S. You, Z. B. Lei, G. H. Zhou, J. J. Yang, G. P. Wu, G. J. Ma, G. Y. Luan, T. Takata, M. Hara, K. Domen, C. Li, Chem. Commun **19**, 2192 (2004).
[8] S. W. Liu, J. G. Yu, M. Jaroniec, Chem. Mater **23**, 4085 (2011).
[9] A. Kubacka, M. Femandez-Garcia, G. Colon, Chem. Rev **112**, 1555 (2012).
[10] M. Romero, J. Blanco, B. Sanchez, A. Vidal, S. Malato, A. I. Cardona, E Garcia, Solar Energy **66**, 169 (1999).
[11] A. Kudo, K. Omori, H. Kato, J. Am. Chem. Soc **121**, 11459 (1999).
[12] A. Walsh, Y. F. Yan, M. N. Huda, M. Al-Jassim, S. H. Wei, Chem. Mater **21**, 547 (2009).
[13] Z. Y. Zhao, Z. S. Li, Z. G. Zou, Phys. Chem. Chem. Phys **13**, 4746 (2011).
[14] L. Zhang, D. R. Chen, X. L. Jiao, J. Phys. Chem. B **110**, 2668 (2006).
[15] A. P. Zhang, J. Z. Zhang, J. Z. Mater. Lett **63**, 1939 (2009).
[16] Y. H. Ng, A. Iwase, A. Kudo, R. J. Amal, Phys. Chem. Lett **1,** 2607 (2010).
[17] W. Z. Wang, M. Shang, W. Z. Yin, R. Jia, Z. Lin, J. Inorg. Mater **27**, 11 (2012).
[18] S. Tokunaga, H. Kato, A. Kudo, Chem. Mater **13**, 4624 (2001).
[19] X. Meng, L. Zhang, H. X. Dai, Z. X. Zhao, R. Z. Zhang, Y. X. Liu, Mater. Chem. Phys **125**, 59 (2011).
[20] Y. F. Sun, Y. Xie, C. Z. Wu, R. Long, Cryst. Growth Des **10**, 602 (2010).
[21] H. Fan, T. Jiang, H. Y. Li, D. J. Wang, L. L. Wang, J. L. Zhai, D. Q. He, P. Wang, T. F. Xie, J. Phys. Chem. C **116**, 2425 (2012).
[22] L. Zhou, W. Z. Wang, S. W. Liu, L. S. Zhang, H. L. Xu, W. Zhu, J. Mol. Catal. A:Chem **252**, 120 (2006).
[23] Y. Guo, X. Yang, F. Y. Ma, K. X. Li, L. Xu, X. Yuan, Y. H. Guo, Appl. Surf. Sci **256**, 2215 (2010).
[24] T. Lu, B. C. H. Steele, Solid State Ionics **21**, 339 (1986).
[25] U. M. G. Perez, S. Sepulveda-Guzman, A. M. L. Cruz, U. O. Mendez, J. Mol. Catal.A:Chem **335**,169 (2011).
[26] J. Yu, A. Kudo, Adv. Funct. Mater **16**, 2163 (2006).

[27] U. M. G. Perez, S. Sepulveda-Guzman, A. M. L. Cruz, Solid State Sci **14**, 293 (2012).
[28] N. C. Castillo, A. Heel, T. Graule, C. Pulgarin, Appl. Catal. B:Environ. **95**, 335 (2010).
[29] S. S. Dunkle, R. J. Helmich, K. S. Suslick, J. Phys. Chem. C **113**, 11980 (2009).
[30] W. Z. Yin, W. Z. Wang, L. Zhou, S. M. Sun, L. Zhang, J. Harzard. Mater **173**, 194 (2010).
[31] A. P. Zhang, J. Z. Zhang, N. Y. Cui, X. Y. Tie, Y. W. An, L. J. Li, J. Mol. Catal. A: Chem **304**, 28 (2009).
[32] P. Madhusudan, J. R. Ran, J. Zhang, J. G. Yu, G. Liu, Appl. Catal. B **110**, 286 (2011).
[33] L. Zhou, W. Z. Wang, L. S. Zhang, H. L. Xu, W. Zhu, J. phys. Chem. C **111**, 13659 (2007).
[34] G. Q. Tan, L. L. Zhang, H. J. Ren, S. S. Wei, J. Huang, A. Xia, ACS Appl Mater interfaces **5**, 5186 (2013).
[35] S. Tokunaga, H. Kato, A. Kudo, A. Chem. Mater **13**, 4624 (2001).
[36] S. Poulston, N. J. Price, C. Weeks, M. D. Allen, P. Parlett, M. Steinberg, M. Bowker, J. Catal **178**, 658 (1998).
[37] H. Y. Kang, S. N. Lim, S. B. Park, Int. J. Hydrogen Energy **37**, 4026 (2012).
[38] H. Y. Fan, G. N. Wang, L. L. Hu, Solid state sciences **11**, 2065 (2009).
[39] Y. Shimizugawa, N. Sugimoto, K. Hirao, J. Non-Cryst. Solids **221**, 208 (1997).
[40] S. L. T. Anderson, J. Chem. Soc. Faraday Trans **75**, 1356 (1979).
[41] Y. X. Liu, H. X. Dai, J. G. Deng, L. Zhang, C. T. Au, Nanoscale **4**, 2317 (2012).
[42] K. J. Tabata, Y. K. Hirano, E. J. Suzuki, Appl. Catal. A **170**,245 (1998).
[43] Y. B. Wan, S. H. Wang, W. H. Luo, L. H. Zhao, Int. J. Photoenergy. (2012) doi:10.1155/2012/392865.
[44] S. W. Cao, Z. Yin, J. Barber, F. Y. C. Boey, S. C. J. Loo, C. Xue, ACS Appl. Mater. Interfaces **4**,418 (2012).
[45] S. M. Sun, W. Z. Wang, L. Zhou, H. L. Xu, Ind. Eng. Chem. Res **48**,1735 (2009).
[46] H. Y. Jiang, X. Meng, H. X. Dai, J. G. Deng, Y. X. Liu, L. Zhang, Z. X. Zhao, J. Hazard. Mater **217-218**, 92 (2012).

*Corresponding author: wangxiansheng728@sina.com